

# The globular cluster systems of 54 Coma ultra-diffuse galaxies: statistical constraints from *HST* data

N. C. Amorisco<sup>1,2\*</sup>, A. Monachesi<sup>1</sup>, S. D. M. White<sup>1</sup>

<sup>1</sup>*Max Planck Institute for Astrophysics, Karl-Schwarzschild-Strasse 1, 85748 Garching, Germany,*

<sup>2</sup>*Institute for Theory and Computation, Harvard-Smithsonian Center for Astrophysics, 60 Garden St., MS-51, Cambridge, MA 02138, USA*

14 April 2022

## ABSTRACT

We use data from the *HST* Coma Cluster Treasury program to assess the richness of the Globular Cluster Systems (GCSs) of 54 Coma ultra-diffuse galaxies (UDGs). This increases the number of cluster UDGs with well characterised GCSs from 3 to 54, 18 of which have a half-light radius exceeding 1.5 kpc. We use a maximum-likelihood method tested on a large number of mock datasets to account consistently for the high and spatially varying background counts in Coma. We find no candidate for a GCS as rich as that of the Milky Way – the highest upper limit (90% confidence) corresponds to  $M_{\text{vir}} < 2.0 \times 10^{11} M_{\odot}$  for the standard relation between GCS richness and halo mass. We assess the statistical significance of any mismatch between the measured GC abundances and those expected for ‘normal’ dwarf galaxies of the same stellar mass. Our population of UDGs shows no evidence for enhanced GCS richness. A stacking analysis of the 18 largest UDGs shows that enhancement by a factor greater than 2.3 is excluded at 90% confidence.

**Key words:** galaxies: dwarf — galaxies: structure — galaxies: formation — galaxies: haloes — galaxies: clusters

## 1 INTRODUCTION

Ultra-diffuse galaxies (UDGs) are a population of low-surface brightness systems (effective surface brightness  $\langle \mu \rangle_r \gtrsim 24$  mag/arcsec<sup>2</sup>) with stellar masses typical of dwarf galaxies ( $7 \lesssim \log M_*/M_{\odot} \lesssim 9$ ). Ubiquitous in nearby galaxy clusters (van Dokkum et al. 2015; Koda et al. 2015; Muñoz et al. 2015; van der Burg et al. 2016; Mihos et al. 2015), UDGs have also been found outside cluster environments (Martinez-Delgado et al. 2016; Roman & Trujillo 2016; Trujillo et al. 2017; Bellazzini et al. 2017). In clusters, they appear as roundish featureless spheroids (e.g. Yagi et al. 2016), which extend the red sequence of cluster galaxies in the colour-magnitude diagram into the regime of dwarf galaxies (Koda et al. 2015; van der Burg et al. 2016), with hints of a trend to bluer colours in less dense environments (Roman & Trujillo 2016).

UDGs are certainly highly dark matter dominated systems (van Dokkum et al. 2015; Beasley et al. 2016; Amorisco & Loeb 2016; van Dokkum et al. 2016), and particular interest has been sparked by the mismatch between their luminosity and their sizes, prompting the proposal that their halo mass could be much larger than suggested by their stellar mass (van Dokkum et al. 2015; Koda et al. 2015;

van Dokkum et al. 2016). Within this scenario, UDGs are prematurely quenched galaxies, which ‘fail’ to form their stars because of their early infall onto the galaxy cluster (Yozin & Bekki 2015; van Dokkum et al. 2015). The largest UDGs (e.g. half-light radii  $\gtrsim 1.5$  kpc) could then be hosted by Milky Way (MW) mass haloes rather than by haloes with masses below or similar to that of the Large Magellanic Cloud (LMC).

One clue to the nature of UDGs which has not been sufficiently explored so far is the almost perfect linearity of the relation between the abundance of UDGs in clusters and the cluster mass itself (van der Burg et al. 2016). This indicates that UDGs are an approximately constant fraction of cluster populations, showing little additional dependence on cluster richness, and by extension on local environment. In contrast with the scenario above, this suggests that the physical mechanism that gives UDGs their unusual properties has an ‘internal’ origin, and is unrelated to the interaction with the cluster environment. This is corroborated by the detection of UDGs outside cluster cores (Martinez-Delgado et al. 2016; Roman & Trujillo 2016) and in the field (Trujillo et al. 2017; Bellazzini et al. 2017).

If hosted by MW mass haloes, UDGs would lie far from the standard  $qM_* - M_{\text{vir}}$  relation, requiring their formation pathway to differ fundamentally from that of ‘normal’ haloes of the same total mass. In general, haloes of MW

\* E-mail: nicola.amorisco@cfa.harvard.edu

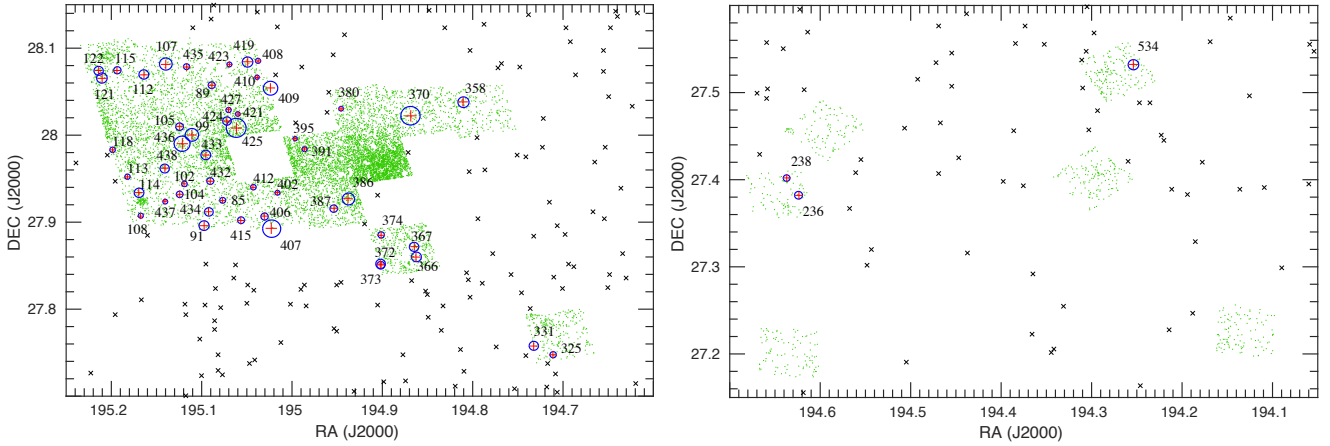


**Figure 1.** A composite of the *HST*/ACS fields observed as part of the Coma Cluster Treasury programme, together with the Coma UDGs from Yagi et al. (2016), shown as black and red crosses. Green points are candidate GCs selected from the Hammer et al. (2010) catalog, as described in Sect. 2.1. The 54 UDGs whose centres fall within the observed *HST* fields are marked in red, their size is shown by a blue circle (with a radius of  $6 \times R_S$ ), and their ID number in the Yagi et al. (2016) catalogue is displayed.

mass appear to be the most efficient at converting gas into stars (e.g. Guo et al. 2010; Behroozi et al. 2013; Moster et al. 2013, and references therein) so the UDG haloes would have to be exceptional objects with very low efficiency. If on the other hand UDG haloes are similar in mass to those of normal dwarf galaxies, their properties could be accommodated by a simple  $\Lambda$ CDM framework in which they are just the low surface brightness tail of the abundant population of dwarf galaxies (Amorisco & Loeb 2016). This picture is consistent with UDGs existing both inside and outside clusters and needs no *ad hoc* mechanism to make them depart from the  $M_* - M_{\text{vir}}$  relation. Additionally, if hosted by low mass haloes, stellar feedback during their formation might lead to expansion and so contribute to their large sizes (Di Cintio et al. 2016).

Unfortunately, only three halo masses are so far available for UDGs. These are all indirect, based either on the richness of the globular cluster system (GCS), or on extrapolation to the virial radius of a dynamical mass estimated in the main stellar body of the galaxy (Beasley et al. 2016; Beasley & Trujillo 2016; Peng & Lim 2016; van Dokkum et al. 2016). Both techniques have their limitations. The approximate linearity of the relation between GCS richness and halo virial mass is supported by a solid pool of evidence, at least for ‘normal’ galaxies (e.g., Harris et al. 2013; Hudson et al. 2014; Forbes et al. 2016, and references therein), but the mean conversion factor remains uncertain (Harris et al. 2015; Zaritsky et al. 2016; Harris et al. 2017; Georgiev et al. 2010, hereafter G10). Dynamical measurements, however, do not guarantee higher precision, as the extrapolation from the galaxy’s half-light radius to the virial radius is very substantial (e.g. Walker et al. 2009; Wolf et al. 2010; Amorisco & Evans 2011; Campbell et al. 2016).

In this Letter, we increase the number of virial mass estimates for UDGs by over an order of magnitude by using imaging data from the *HST* Coma Cluster Treasury program to constrain the richness of the GCS of 54 Coma UDGs. In comparison to ground-based data, the high resolution of *HST*/ACS data help significantly in distinguishing candidate GCs from background galaxies (e.g., Peng et al.

2011; Beasley & Trujillo 2016; Peng & Lim 2016). However, the relatively poor GCSs of these UDGs together with the high contamination rate by GCs associated with other cluster galaxies and with the intracluster population imply that careful statistical analysis is needed to gather reliable constraints. Sect. 2 describes the data we use for this analysis. Sect. 3 sets out and tests our maximum-likelihood approach. Sect. 4 presents our results, and Sect. 5 lays out our conclusions.

## 2 OBSERVATIONS AND METHODS

We use the compilation of 854 Coma UDGs presented by Yagi et al. (2016, hereafter Y16), based on Subaru Suprime Cam archival data analysed in Koda et al. (2015). These are selected to have  $\langle \mu \rangle_R > 24$  mag/arcsec<sup>2</sup> and a stellar half light radius  $\geq 0.7$  kpc. Among these, we select those UDGs whose centers lie within the footprint of the Coma Cluster Treasury program, which we use to explore the properties of their GCSs. There are 54 such UDGs. Their locations are displayed in Fig. 1, together with their ID numbers in the Y16 catalog. We adopt half-light radii  $R_S$  from the single Sersic fits presented by Y16. Where these were not deemed reliable, for example because of light from nearby systems, we adopt the listed values returned by SExtractor.

### 2.1 Candidate GC selection

We cross-correlate the position of the Y16 UDGs with the catalog of the *HST*/ACS Coma Cluster Treasury program (CCTp) presented by Hammer et al. (2010, hereafter H10). This lists all SExtractor sources detected in the deep *F*814W images, as well as the measurements for the *F*475W images, and we use it to select GC candidates (GCCs) within the footprint of the survey. AB magnitude system photometry is available at different apertures (*HST*/ACS imaging has  $0.''05/\text{pixel}$ ): we use the 4 pixel radius aperture ( $0.''2$ ) and apply the aperture corrections from Sirianni et al. (2005). We correct magnitudes for Galactic extinction following

Schlafly & Finkbeiner (2011), using the E(B-V) reddening values from Schlegel et al. (1998). The  $F814W$ -band photometry is 80% and 50% complete at 26.8 and 27.3, respectively (H10 and Peng et al. 2011). This defines our completeness function  $S_{814}$ , for which we adopt the functional form suggested by Salinas et al. (2015, eqn. 3, resulting in  $\alpha = 1.5$ ). Assuming UDGs have a dwarf-like GC luminosity function (GCLF), CCTp data is therefore  $\approx 50\%$  complete at the turnover,  $F814W = 27.33$  mag, (Miller & Lotz 2007; Peng et al. 2011; Beasley & Trujillo 2016). If the spread of the GCLF is also in line with that of dwarf galaxies (Gaussian spread of 1.1 mag), statistically,  $\approx 40\%$  of all member GCs are indeed detected in the CCTp data.

*HST*/ACS imaging is well suited to disentangle GCCs (which appear as point sources at the distance of Coma) from background galaxies, most of which are resolved. We first select objects flagged as ‘point sources’ in the H10 catalogue (FLAGS\_OBJ=1). We then constrain the concentration index  $C_{4-10}$ , defined here as the difference in magnitude between a 4- and a 10-pixel aperture radius, following a similar approach to that of Peng et al. (2011) and Beasley & Trujillo (2016). True point sources lie at  $C_{4-10} = 0.13$  in the absence of noise, as shown in Figure 2. Using the concentration index and  $F814W$  magnitudes, we generate a sample of GCCs by selecting all objects within  $\pm 0.2$  mag of  $C_{4-10} = 0.13$  and with  $F814W < 27.3$ . In addition, we apply a colour cut,  $0.5 < F475W - F814W < 1.5$ , in order to exclude compact red galaxies (Peng et al. 2011; Beasley & Trujillo 2016), and we impose a bright magnitude limit of  $F814W > 22$  to avoid foreground MW stars and saturated pixels (H10). Finally, we use the celestial coordinates of the sources to eliminate all duplicate detections resulting from our combining of the catalogues for the 25 *HST*/ACS fields observed in the CCTp. The final catalogue contains  $\sim 12000$  GCCs.

### 3 STATISTICAL ANALYSIS

As shown by Peng et al. (2011) using these same data, the Coma cluster possesses an abundant population of intracluster GCs (ICGs), and, in addition, several tens of background galaxies survive the above selection in each ACS field. As is readily seen by eye, the CCTp distribution of GCCs displays clear overdensities at the locations of high surface brightness Coma galaxies (see Fig. 1 and 3 in Peng et al. 2011). In contrast, and despite our above estimate of the depth of the CCTp data, visual inspection rarely reveals any apparent concentration of GCCs near the UDG centers: it appears that UDGs typically have poor GCSs relative to the background. As a result, we cannot reliably measure their GC abundances simply by counting GCCs within some centred aperture and then subtracting an estimate for the background contamination. A more detailed statistical approach, which we describe in the following, is necessary to constrain the richness,  $N_{GC}$  of the GCSs of our UDG sample.

#### 3.1 The mixture models

We isolate the GCCs in the vicinity of each UDG, and model them as the superposition of a slowly spatially varying population of contaminants and a centred population of GCs physically associated with the UDG. In the absence

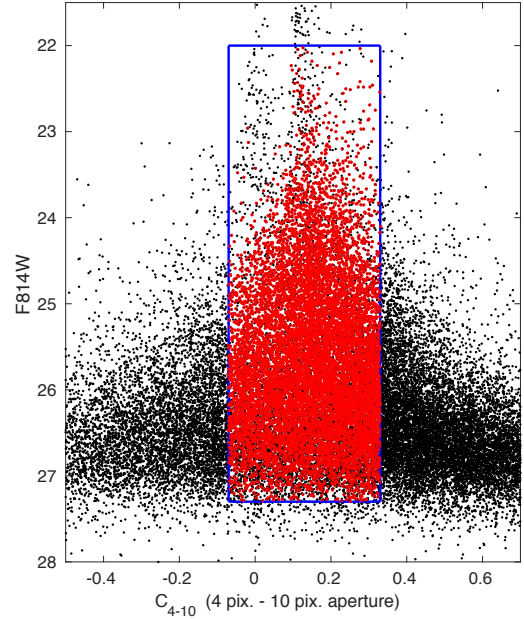


**Figure 2.** Point sources in the CCTp selected as GC candidates. The blue box indicates the cuts applied in  $F814W$  magnitude and concentration index  $C_{4-10}$ , defined as the difference in magnitude between a 4- and a 10-pixel aperture radius. Red points also satisfy the adopted color cut.

of close luminous galaxies, we apply this model to all GCCs within  $35 \times R_S$  from the UDG’s center. This is a compromise between getting better statistics for the contaminants and modelling their spatial distribution as locally uniform, with surface density  $\Sigma_c$ . When near luminous galaxies, we reduce this region on a case by case basis in order to minimise spatially variable contamination (see below and Fig. 4). For convenience, we center all GCCs’ coordinates on the UDG’s center, and rescale them by the stellar half-light radius  $R_S$ . The spatial distribution of the UDG GCS is modelled with a Plummer profile (Plummer 1911)

$$\Sigma(R) = \frac{1}{\pi} \frac{1}{R_h^2 (1 + R^2/R_h^2)^2}, \quad (1)$$

in which the ratio between the half-count radius  $R_h$  and the stellar half-light radius  $R_S$  is a free parameter. Experiments using an exponential density profile  $\Sigma$  show that the profile shape does not affect our results much, as we do not detect enough members to fully characterise the density profile of the GCS (see also the results of our tests in Sect. 3.2).

Our simplest mixture model, *model 1*, uses only the spatial distribution of the GCCs to separate member GCs and contaminants. Following Walker & Peñarrubia (2011) and Amorisco et al. (2014), the likelihood of observing a sample of  $N$  GCCs at distances  $\mathbf{r}_i$  from the UDG is

$$\mathcal{L}_1 = \prod_i^N \left[ f \frac{S_{sp}(\mathbf{r}_i) \Sigma(r_i, R_h/R_S)}{\int S_{sp} \Sigma(r, R_h/R_S)} + (1 - f) \frac{S_{sp}(\mathbf{r}_i)}{\int S_{sp}} \right], \quad (2)$$

with free parameters  $f$  and  $R_h/R_S$  ( $\Sigma_c$  cancels out). Here,

- $S_{sp}(\mathbf{r})$  is the spatial selection function, whose value is either 0 or 1. This function accounts for the fact that the area available to study may be limited by the edges of the

footprint, or by excised regions surrounding luminous galaxies, in which case its value is 0.

- $f$  is the fraction of the total number  $N$  of GCCs in the studied area which are associated with the UDG.
- The spatial integrals extend out to  $35 R_S$ .

A second mixture model, *model 2*, uses in addition the candidates'  $F814W$  magnitude,  $m$ , to help distinguish member GCs from contaminants. The likelihood function then takes the form

$$\mathcal{L}_2 = \prod_i^N \left[ f \frac{S_{\text{sp}}(\mathbf{r}_i) \Sigma(r_i, R_h/R_S)}{\int S_{\text{sp}} \Sigma(r, R_h/R_S)} \frac{S_{814}(m) g_{GC}(m)}{\int S_{814} g_{GC}} + (1-f) \frac{S_{\text{sp}}(\mathbf{r}_i)}{\int S_{\text{sp}}} \frac{S_{814}(m) g_c(m)}{\int S_{814} g_c} \right]. \quad (3)$$

Here,

- $S_{814}$  is the completeness function we have characterised in Sect. 2;
- $g_{GC}$  is the luminosity function of the member GCs;
- $g_c$  is the luminosity function of the contaminants.
- The second integral in each denominator is over magnitude,  $m$ .

Since we do not expect the GCSs of our UDGs to be rich enough to fully characterise  $g_{GC}$  (see Sect. 3.2), we adopt a fixed Gaussian GCLF,  $\mathcal{G}$ , with parameters typical for dwarf galaxies: a mean of  $\langle F814W \rangle = 27.33$  mag, and a spread of  $\sigma_{F814W} = 1.1$  mag (G10, Miller & Lotz 2007; Peng et al. 2009). Since modelling explicitly the magnitude distribution of the contaminants  $g_c$  would require us to make hypotheses for all its different components (ICGs, background galaxies, foreground stars, etc.) and/or to introduce new free parameters into our model, we adopt a simpler approach, based on the fact that, as our results will show, contaminants represent  $\gtrsim 99\%$  of the sources in our catalogue of GCCs. It follows that the product  $S_{814} g_c$  is well described by the observed magnitude distribution of the full catalogue of candidates. We therefore fix it in *model 2* by using this empirically determined distribution. The tests described in Sect. 3.2 demonstrate this is a useful working assumption. In conclusion, this second mixture model uses both candidates' spatial distribution and magnitudes, but in fact does not introduce additional free parameters with respect to *model 1*. We discuss and define the priors that we use in Sect. 3.2.2.

Both mixture models allow us to infer the joint posterior distribution of the two dimensionless free parameters  $f$  and  $R_h/R_S$  which characterise each GCS. Our final inference on the total abundance of the GCS,  $N_{GC}$ , is obtained by taking into account both spatial and magnitude incompleteness:

$$N_{GC,j} = N f_j \times \frac{\int \Sigma(r, R_{h,j}/R_S)}{\int S_{\text{sp}}(\mathbf{r}) \Sigma(r, R_{h,j}/R_S)} \frac{\int \mathcal{G}(m)}{\int S_{814} \mathcal{G}(m)}, \quad (4)$$

where  $j$  runs over our Markov chains. It is worth noting that the turnover and spread of the GCLF become respectively fainter and tighter in dwarf galaxies (e.g. Jordán et al. 2007). Therefore, our assumptions on the properties of  $g_{GC}$  are conservative: for the same values of  $f$  and  $N$ , the corrected GC richness of a dwarf galaxy is higher than in bright galaxy.

### 3.1.1 Stacks

As an alternative to studying each UDG individually, stacks are useful to help circumvent the large  $\sim \sqrt{N}$  Poisson uncertainty arising from the dominant background counts. We have already homogenised the spatial distribution of candidates associated with any UDG by centering on the UDG's coordinates, and by rescaling by the UDG's half-light radius  $R_S$ . Consider then a set of  $n$  UDGs surrounded by a total of  $N_{\text{tot}}$  GCCs. Both likelihoods (2) and (3) can be used to study this stack, under the assumption that all systems have a similar  $R_h/R_S$ . The statistical framework described above then provides a measurement of: (i) the fraction  $f$  between the total number of GCs physically associated with any of the stacked UDGs,  $N_{\text{memb,tot}}$  and the total number of candidates over the stack,  $N_{\text{tot}}$ ; (ii) an 'average' value for the size of the GCSs,  $\langle R_h/R_S \rangle$ . The tests we perform on mock datasets and describe in Sect. 3.2 show that  $\langle R_h/R_S \rangle$  is compatible with the straight average of the input values; after correction as in eqn. (4),  $N_{\text{memb,tot}}/n$  is compatible with the straight average of the input abundances,  $\langle N_{GC} \rangle$ .

The only quantity that requires additional discussion is the spatial selection function. By definition, the spatial selection function quantifies the fraction of actually observed candidates. For individual UDGs, this only takes values 1 or 0, corresponding respectively to regions that are in the available footprint, and regions that are not, or are excised. The combined spatial selection function of a stack,  $S_{\text{sp,st}}$ , is constructed as follows:

$$S_{\text{sp,st}}(\mathbf{r}) \equiv \sum_j^n \Sigma_{c,j} S_{\text{sp,j}}(\mathbf{r}) \approx \sum_j^n \frac{N_j}{\int S_{\text{sp,j}}(r)} S_{\text{sp,j}}(\mathbf{r}). \quad (5)$$

Here, the index  $j$  runs on the  $n$  UDGs in the stack, and  $\Sigma_{c,j}$  is the uniform density of contaminants associated with the  $j$ -th UDG, after spatial rescaling. Eqn (5) has a straightforward interpretation: in those regions of the stack that are not within the footprint available for the  $j$ -th UDG,  $S_{\text{sp,j}} = 0$ , a fraction of candidates proportional to  $\Sigma_{c,j}$  is lost. The second part of eqn. (5) provides an operational estimate for  $S_{\text{sp,st}}$ , again based on the strong dominance of the contaminant population. We refer to Section 3.2 for tests of this approximation.

We will consider 4 different stacks:

- two combine UDGs based on their size, stacking the 18 systems with  $R_S > 1.5$  kpc, and the complementary sample of 36;
- two combine UDGs based on their stellar mass, stacking the 18 systems with  $\log M_*/M_\odot > 7.5$ , and the complementary sample of 36. Note that the 18 largest UDGs are not the 18 with the highest stellar mass. The bound  $\log M_*/M_\odot > 7.5$  was chosen so that our second pair of stacks would have the same number of UDGs.

### 3.2 Test suites

Here we test our statistical framework, using purposely generated mock UDG datasets. We have a series of objectives. First, we wish to evaluate our method's performance, in particular, when applied to data with the properties of the CCTp data. Second, we wish to determine the prior distributions that are most appropriate for this study, and to



explore any biases they might give rise to. Third, we will use mock UDG data sets with known input properties to contextualise measurements based on the real data. Specifically, the GCS of any given UDG is compatible with a particular set of properties if our methods produce indistinguishable results when applied to the real data and to mock datasets generated according to those properties. This procedure can also be used to assess the statistical significance of any mismatch between the CCTp data for a given UDG and some particular set of properties. For example, in Sect. 3.2.3 we use this method to compare the properties of our 54 UDGs with those of ‘normal’ galaxies with the same stellar mass.

### 3.2.1 UDG mock datasets as ‘normal’ dwarfs

For each of our 54 UDGs, we generate a set of 100 mock datasets with the same footprint as the real data, and therefore the same spatial selection function. Mock datasets comprise a population of member GCs and a population of contaminants. The contaminant population is uniformly distributed with surface density  $\Sigma_{c,j}$ , estimated using the real data as in eqn (5). A magnitude for each contaminant source is generated from the magnitude distribution  $g_c$ , estimated as described in Sect. 3.1.

The mock member GCs are generated using the following model.

- The total richness of the GCS,  $N_{GC}$ , depends only on the stellar mass of the UDG,  $M^*$ , and has a Poisson distribution around the mean relation

$$\log N_{GC,0} = 0.58 \log(M^*/M_\odot) - 4.09, \quad (6)$$

with no intrinsic scatter. This relation provides the best linear fit in log-log space to the properties of the sample constructed by Georgiev et al. (2008, 2009, 2010), which collects  $> 50$  nearby dwarf galaxies observed with HST (see Fig. 7). Stellar masses for all our UDGs are obtained assuming that  $B - R \sim 1$  for the UDGs (Koda et al. 2015), and averaging between the  $M/L$  relations of Zibetti et al. (2009) and Bell et al. (2003). Final values are listed in Table 1.

- The GCS has a Plummer or an exponential spatial distribution, each with a probability  $p = 0.5$ . Note that both *model 1* and *model 2* assume a Plummer density distribution. This allows us to test how the uncertainty on the actual profile of the UDG GCS affects our results. For either Plummer or exponential profiles, the half-count radius  $R_h$  has a Gaussian distribution with mean  $R_h/R_S = 1.8$  and a scatter of 0.3. We reckon this is a reasonable assumption, encompassing the properties of normal galaxies (e.g., Kartha et al. 2014; Caldwell & Romanowsky 2016), as well as of UDGs studied so far (Beasley et al. 2016; Peng & Lim 2016; van Dokkum et al. 2016).

- A magnitude value for each member GC is generated assuming the GCS has a Gaussian luminosity function, with values typical for normal dwarf galaxies (G10, Miller & Lotz 2007; Peng et al. 2009). Different mock datasets, however, have different GCLF: individual turnovers and spreads are centered respectively in  $\langle F814W \rangle = 27.33$  mag and  $\sigma_{F814W} = 1.1$  mag, and have a Gaussian distribution around these values with a scatter of 0.1 mag. Note that results obtained from the mock datasets are also corrected for incompleteness through eqn (4), in which we have assumed

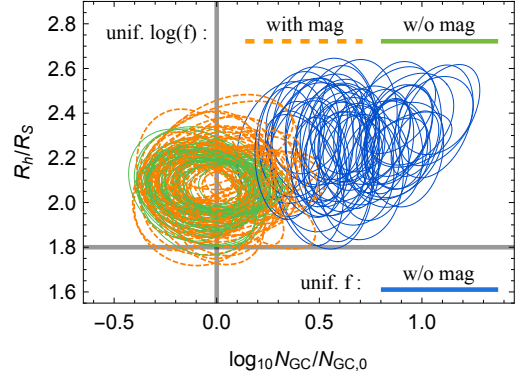


**Figure 3.** Performance of our statistical framework. Horizontal and vertical lines indicate the mean input parameters used to generate the mock datasets (a set of 100 for each UDG). For each UDG, coloured ellipses show the 1-sigma regions for the distributions of measurements on mock data (median GC abundance  $N_{GC}$ , median half-count radius  $R_h/R_S$ ). The mismatch between ellipses and gray lines quantifies bias. Solid ellipses correspond to results obtained using *model 1*: in blue when adopting a prior with uniform density in  $f$ , in green if the prior has uniform density in  $\log f$ . Orange dashed ellipses refer to *model 2* and to a prior with uniform density in  $\log f$ .

fixed values for  $\langle F814W \rangle = 27.33$  and  $\sigma_{F814W} = 1.1$ . As for the density profile of the GCS, this allows us to explore the effect that the uncertainty on the UDG GCLF has on our measurements.

The populations of both contaminants and members are then filtered by the same spatial and magnitude selections that characterise the CCTp data. For each UDG, spatial selection excises all those mock GCCs that fall outside the available footprint, or in excised areas. Magnitude selection excises with probability  $p = 1 - S_{814}(m)$  mock candidates with  $F814W$  magnitude  $m$ .

For each UDG, these steps produce mock datasets that mimic the GCS of a ‘normal’ dwarf galaxy having the same stellar mass. This includes some residual variability, connected with the following uncertainties:

- the Poisson noise on  $N_{GC,0}$ , connected to the discrete nature of GCs,
- the uncertainty on the precise density profile of the GCS;
- the uncertainty on the detailed parameters of the GCLF;
- the intrinsically statistical nature of the magnitude selection.

These introduce scatter in our measurements, whose size is important when trying to establish how different UDGs are from ‘normal’ dwarfs, as we show in Sect 3.2.3. Finally, by combining mock datasets pertaining to different UDGs, we can generate mock stacks having the same properties as our real stacks, and so test the performance of our methods for analyzing stacked data.

### 3.2.2 Prior distributions and biases

The main difficulty presented by the data at hand lies in the dominant background counts. This implies that use of prior

distributions that weigh differently the parameter volume  $0 < f < 1$  can influence our inferences. For this reason, we explore two different prior distributions. A uniform prior in  $f$ ,  $0 < f < 1$ , and a uniform prior in  $\log f$ . In the latter case, a finite lower bound is needed, and we use  $\log f_0 - 1.5 < \log f < 0$ , where the value  $f_0$  is the fraction of members expected in the data when  $N_{GC} = N_{GC,0}$ , i.e. if the GCS is ‘normal’, as in eqn. (6).

As to the parameter  $R_h/R_S$ , we test a prior  $0.5 < R_h/R_S < 3.5$ , with uniform distribution. This is suggested by the lack of evidence that the ratio  $R_h/R_S$  of UDGs departs from what common in normal galaxies (Beasley et al. 2016; Peng & Lim 2016; van Dokkum et al. 2016). Furthermore, the prior we consider remains loose, extending up to values that would be considered ‘exotic’ for normal galaxies.

We first test the performance of *model 1*, eqn (2), on all our 54 UDGs, using 100 mock datasets for each them. For each UDG mock dataset, we record results for the median values of the posterior distributions for both  $R_h/R_S$  and  $N_{GC}$ , after correcting the latter for completeness as in eqn (4). Hence, each mock dataset defines a point in this plane. Figure 3 displays the 1-sigma ellipse for the collection of these 100 points, one ellipse for each of our UDGs. Solid ellipses refer to results obtained using *model 1*: blue ellipses use the prior distribution with uniform density in  $f$ , green ellipses refer to the prior distribution with uniform density in  $\log f$ . The horizontal and vertical grey lines display the mean values of the input parameters used to generate the mock datasets: any systematic displacement of the ellipses quantifies bias. It is clear that the prior with uniform density in  $f$  leads to a significant bias in both free parameters: GC abundances are significantly overestimated, by a factor  $\gtrsim 3$ ; the scale radius of the GCS is also overestimated. This is accompanied by a degeneracy between the two free parameters  $f$  and  $R_h/R_S$ , which appears to bias the results.

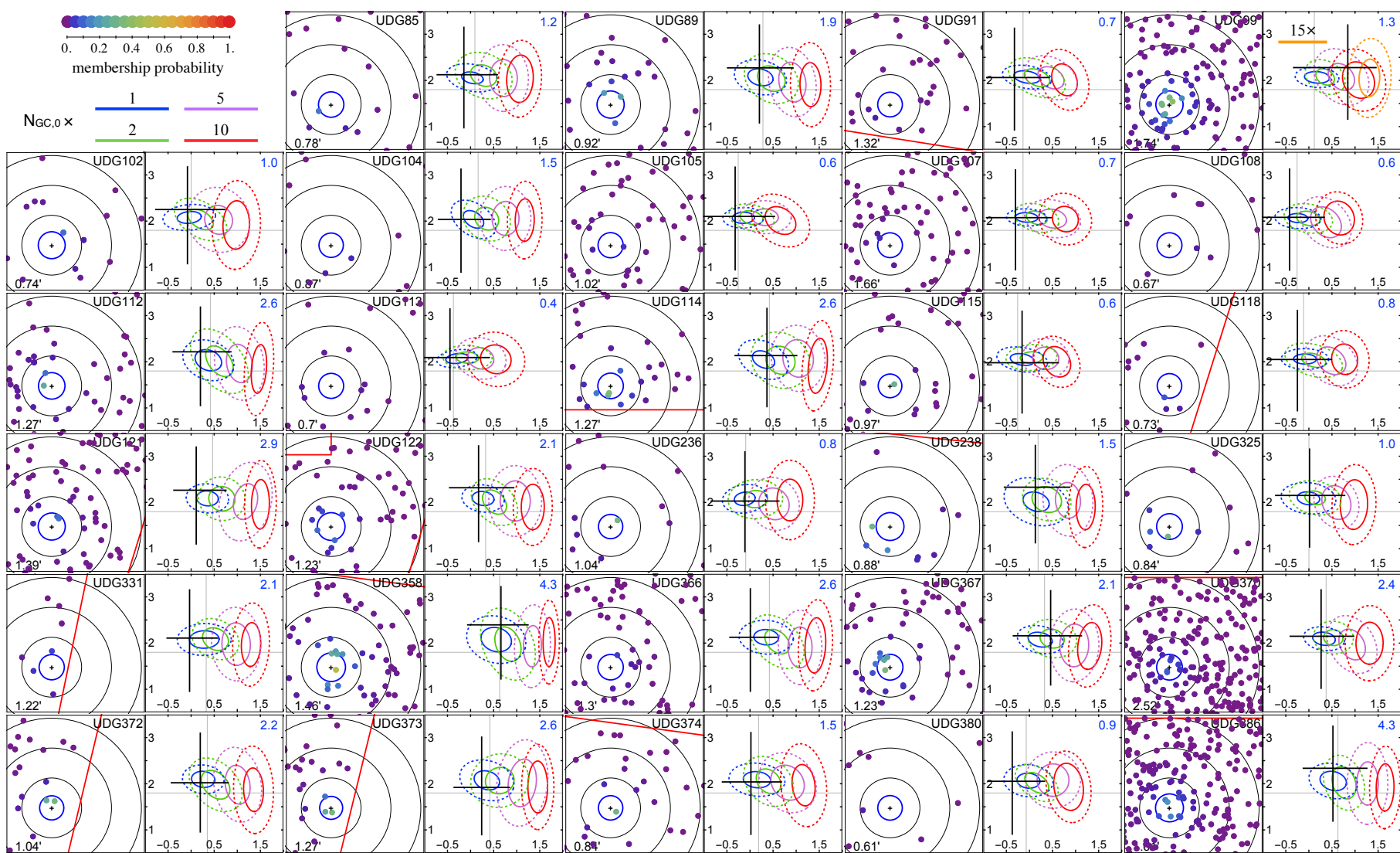
This is significantly ameliorated by adopting the prior distribution with uniform density in  $\log f$ . Some residual bias is still present in our inference for the ratio  $R_h/R_S$ , but we are not concerned by this: all 1-sigma green ellipses are consistent with the target GC abundances  $N_{GC,0}$ . Furthermore, the degeneracy between  $f$  and  $R_h/R_S$  disappears. Therefore, we prefer to avoid enforcing a stronger prior on  $R_h/R_S$ , which may be exceedingly restrictive on the real data.

We also test our *model 2*, to establish whether the additional magnitude information might tighten constraints. We find that results obtained using a uniform prior in  $f$  suffer from the same biases shown by *model 1*. Results obtained using the prior with uniform density in  $\log f$  are shown by orange dashed ellipses in Fig. 3. These do not show systematic improvement with respect to the simpler *model 1*: the magnitude distributions of member GCs and contaminants are not sufficiently different from each other to guarantee a measurable statistical improvement. This is especially the case since the number of member GCs detected with high confidence in each dataset is often vanishingly small, which makes the sampling of the GCLF too sparse to actually help.

Given the result of these tests, in the reminder of the paper we discuss results obtained using *model 1*, in combination with the following priors:

- $\log f_0 - 1.5 < \log f < 0$ , with uniform density;

- $0.5 < R_h/R_S < 3.5$ , with uniform density.



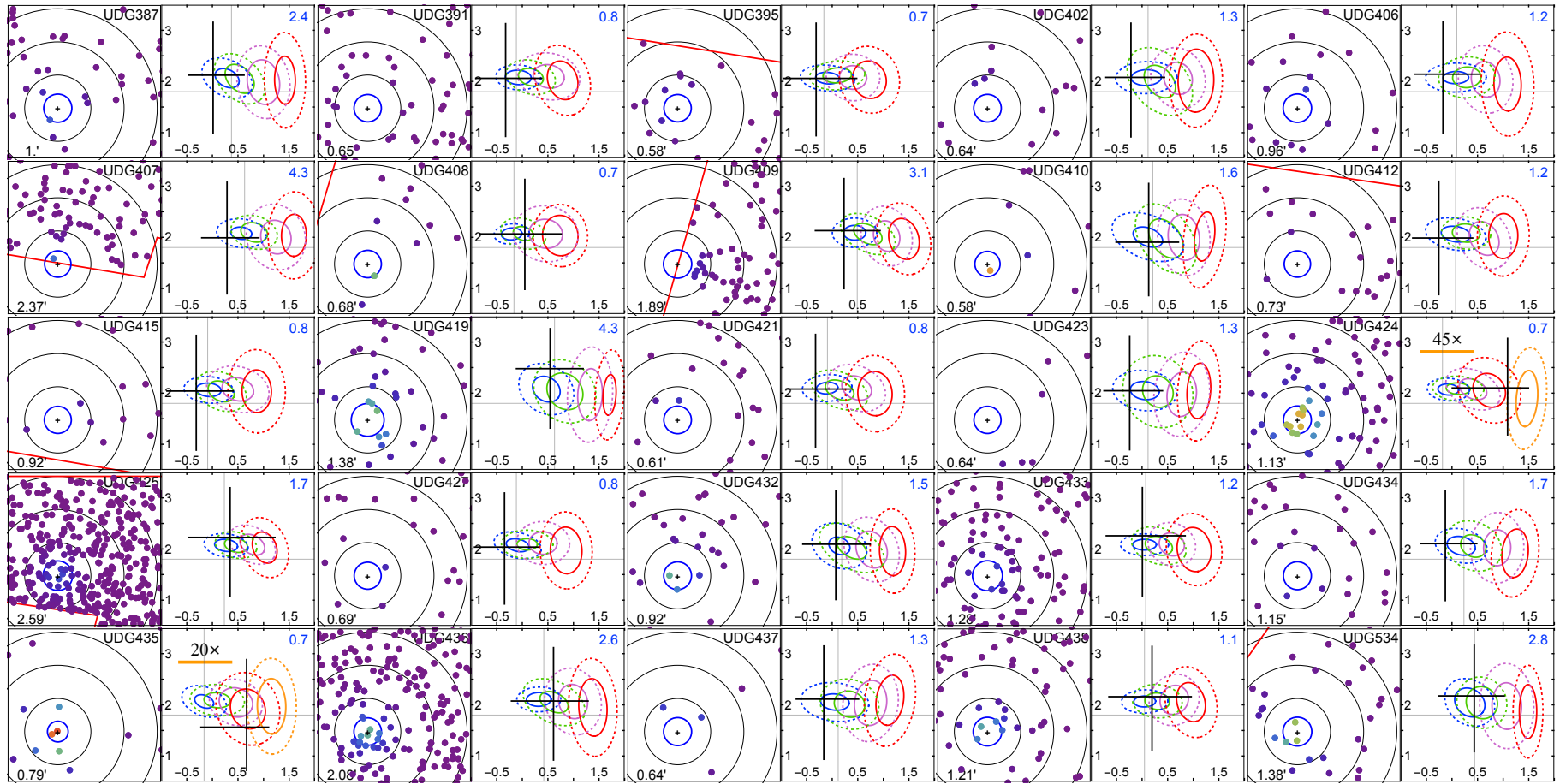


**Figure 4.** Results of the analyses on individual systems. The ID number of each UDG is in the upper-right of the left panel. Left panels show zooms of Fig. 1, with size  $l \times l$ , where  $l$  is indicated in the lower-left of the panel itself. Black concentric circles display  $\{5, 10, 15\} \times R_S$ , the stellar half-light radius of the UDG. The blue circle indicates the median half-counts radius  $R_h$  of the GCS, as obtained from our analysis. Where visible, red lines show the edge of the footprint, or areas excluded due to bright galaxies. Dots are candidate GCs, color-coded by the probability of membership in the UDG, as shown in the legend. The right panels show our inferences for the GC abundance  $N_{GC}$ , after completeness corrections (horizontal axis, units in  $\log N_{GC}$ ), and for the half-count radius of the GC system  $R_h/R_S$  (vertical axis). The black cross extends between the 10 and 90% quantiles of the posterior distribution. The black cross corresponding to mock datasets from models featuring GC abundances of  $\{1, 2, 5, 10\} \times N_{GC,0}$  fall within the ellipses (respectively blue, green, pink and red), which show 1- and 2-sigma regions (solid and dashed ellipses).  $N_{GC,0}$  is the mean GC abundance of ‘normal’ dwarfs with the same UDG stellar mass, its value is displayed in the upper-right of each panel and indicated by the vertical gray line.



### 3.2.3 Different from ‘normal’ dwarfs?

How do we establish if the CCTp data are consistent with UDGs having GCSs of ‘normal’ dwarfs? What is the statistical significance of any mismatch identified? We tackle these questions from both a Bayesian and a frequentist point of view. In a Bayesian interpretation, the posterior distribution we obtain from our maximum likelihood method defines whether that UDG is compatible with a ‘normal’ GC richness. In a frequentist approach we can compare the results of our analysis with those usually obtained when applying the same maximum likelihood technique on mock datasets representing ‘normal’ dwarf galaxies.

In practice, in addition to the models with ‘normal’ abundance presented in Sec. 3.2.1, for each UDG we also consider models with increased abundances, as it may be expected if the virial mass of their haloes are indeed larger than ‘normal’. As done for producing Figure 3, we run our statistical framework on sets of 100 realizations from these models, and record results for the median values of the posterior distributions for both  $R_h/R_s$  and  $N_{GC}$ . Results are collected in Figure 4, in which each UDG is associated to a pair of panels. The right panels ( $\log N_{GC}$  on the horizontal axis and  $R_h/R_s$  on the vertical axis) show the ellipses containing 39% and 86% (solid and dotted) of these medians. Different colors are associated with different GC abundances: 1 (blue), 2 (green), 5 (pink) or 10 (red) times the GC abundance of a normal dwarf galaxy with the same stellar mass,  $N_{GC,0}$ . The value of  $N_{GC,0}$  is displayed in blue in the upper-right of each panel and indicated by the vertical grey line. If the medians of the posterior distributions obtained from the real data fall within the blue ellipses,  $N_{GC} = 1 \times N_{GC,0}$ , the corresponding UDG is compatible with a normal dwarf according to a frequentist interpretation.

A parallel analysis has been performed for our stacks: results for the mean abundance  $\langle N_{GC} \rangle$  and mean scale radius  $\langle R_h/R_s \rangle$  obtained from stacking realizations of ‘normal’ UDGs are displayed as ellipses in Fig. 5. Where necessary, for several individual UDGs and for our stacks, models with increased or decreased abundances have also been considered, to try and bracket the abundance implied by the CCTp data. With reference to the stacked analyses, note that horizontal and vertical solid lines, representing the mean input values, always fall within the blue ellipses, showing that our statistical setup and the associated working assumptions perform very well on stacks.

## 4 RESULTS

### 4.1 Analyses on individual systems

Results for all our 54 UDGs are presented in Fig. 4 and Table 1. Fig. 4 displays zooms of Fig. 1, left panels, concentrating on the central regions, which are placed off-center in order to allow a better impression of the statistics of the contaminants. Each GCC is colour-coded according to its probability of membership in the UDG GCS, obtained from *model 1*. As mentioned earlier, most cases show no obvious over-density of sources close to the center of the UDG, hence the paucity of high-probability members. In several instances, the surface density of contaminants is such that even GCCs located within a few  $R_s$  from the UDG’s center

cannot be considered physically associated with high probability.

The right panel of each pair in Fig. 4 displays our inferences: the black cross extends between the 10% and 90% quantiles of the posterior distributions we obtain for  $N_{GC}$  and  $R_h/R_s$ . The crossing point corresponds to the median values of the two posteriors. Thin grey vertical and horizontal lines show the expected values of  $N_{GC}$  and  $R_h/R_s$  for the reference model of 3.2.1 for the GCSs of normal dwarfs. In only one case (UDG with ID 424) is the expected value of  $N_{GC}$  outside the 10 to 90% range allowed by the data, and in no case is this true for  $R_h/R_s$ . Thus, from a Bayesian point of view, a GCS similar to that of a normal dwarf of similar stellar mass is compatible with all of our individual UDG fields. The same can be inferred from a frequentist point of view by comparing the centres of the black crosses with the blue ellipses. Only in 3 of our 54 cases does the centre fall outside the blue dashed ellipses, which are drawn to contain the centres for 86% of random realisations of the reference model for each system when analysed in the same way as the real data. The number of outliers is thus actually somewhat smaller than expected. The quantiles  $q_i$ , listed in Table 1, quantify the following statement:  $q_i = X$  indicates that the centre of the black cross for the real data lies outside the ellipse containing the centres of 100X% of the realisations of a model with the standard value of  $R_h/R_s$  and  $N_{GC} = i \times N_{GC,0}$ . For two of our 54 systems we find  $q_1 > 0.95$ , for 9 we find  $q_1 > 0.7$  and for 23 we find  $q_1 > 0.5$ , indicating good agreement with standard dwarf GCSs. On the other hand, even for  $i = 2$  we find 30 of 54 systems with  $q_2 > 0.7$  indicating substantially worse agreement, and the disagreement becomes much worse for  $i = 5$  or 10.

The blue number in the upper-right of each panel indicates  $N_{GC,0}$ . The richest expected GCS, as based on the UDGs’ stellar mass, have  $N_{GC,0} = 4.3$ , before Poisson noise. We also recall that the magnitude selection function of CCTp data implies that, statistically,  $\approx 60\%$  of member GCs are not actually detected in the data. This explains the absence of clear overdensities in the distributions of GCCs, as well as the extremely small number of high-probability members identified by our analysis, and visible in Fig. 4.

The three individual cases for which the centre of the black cross lies outside the blue dashed ellipse containing its predicted location for 86% of realisations of our reference GCS model are the UDGs with ID 99, ID 424, and ID 435. For the UDGs with ID 99 and ID 435 the median of the of the posterior distribution is at about 5  $N_{GC,0}$ , and at about 10  $N_{GC,0}$  for the UDGs with ID 424. However,  $N_{GC,0}$  is well within the 10 to 90% range of the posterior distribution for the UDGs with ID 99 and ID 435, and the lower 10% point extends to about 1.4  $N_{GC,0}$  for the UDG with ID 424.

Figure 6 visualises these results. UDGs are ordered by stellar half-light radius  $R_s$  and color coded by stellar mass. Coloured bars are obtained using a frequentist approach, by interpolating the results listed in Table 1, and display the range of values of  $i = N_{GC}/N_{GC,0}$  for which  $q_i < 0.9$ . Empty black rectangles extend between the 10% and 90% quantiles of our marginalised posterior distributions, and therefore refer to a Bayesian interpretation. Corresponding 90% upper limits,  $N_{GC,90}$ , are listed for all UDGs at the top of each panel, with values from a Bayesian approach are on the top. Even when adopting the loosest between these two upper

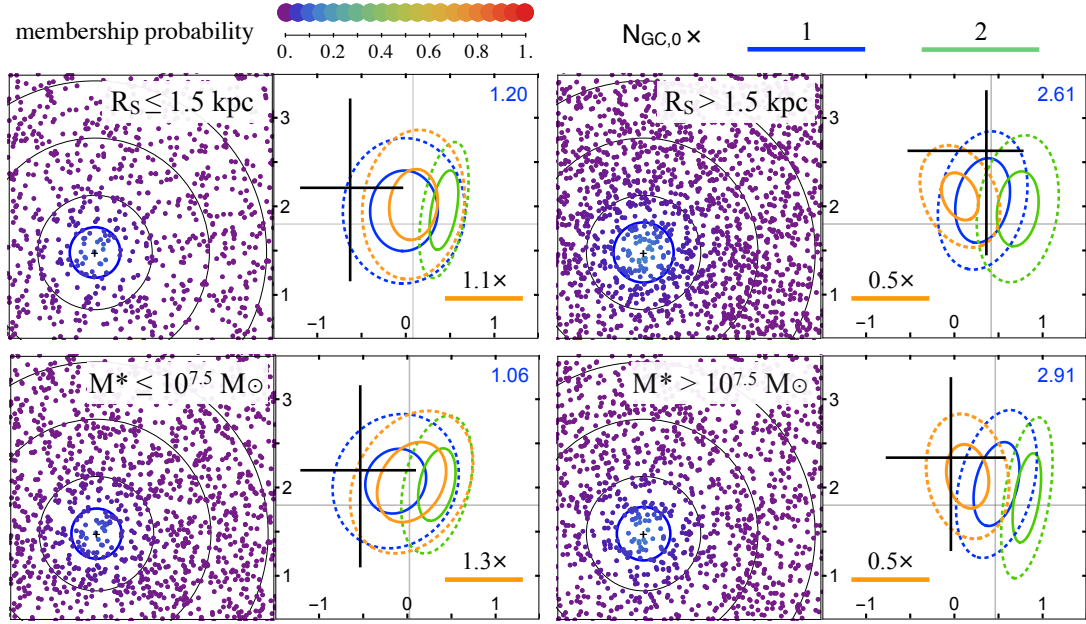


**Figure 5.** Results of the analyses on stacked data: stacks based on size in the top row, stacks based on stellar mass in the bottom row. Both left and right panels are analogous to panels in Fig. 4. Left panels show zooms on the distribution of GCCs, as collected over all stacked UDGs (after spatial rescaling). Each GCC is color-coded by the probability of membership in any of the UDGs in the stack, as shown in the legend. The right panels show our inferences for the mean GC abundance  $\langle N_{GC} \rangle$  (horizontal axis, in units of  $\log \langle N_{GC} \rangle$ ) and mean half-count radius of the GC system  $\langle R_h/R_s \rangle$  (vertical axis), over each sample of stacked UDGs. The black cross extends between 10 and 90% quantiles of the posterior distributions. As in Fig. 4, ellipses show the 1- and 2-sigma regions (solid and dashed ellipses) for the location of the median of the posterior distributions from mocks of models with GC abundances of  $\{1, 2\} \times N_{GC,0}$  (respectively blue and green).  $\langle N_{GC,0} \rangle$  is the mean GC abundance corresponding to a model in which all stacked UDGs are ‘normal’, and its value is displayed in the upper-right of each panel.

limits, in only 6 cases  $N_{GC,90} > 15$ , and of these, only three galaxies have  $N_{GC,90} \geq 20$ . These results show that our 54-strong sample of UDGs is composed by dwarf galaxies.

#### 4.1.1 Upper limits for individual virial masses

We follow Harris et al. (2015), and use GC abundance as a proxy for virial mass. In particular, we interpret values of  $N_{GC,90}$  as upper limits for the virial mass of each UDG,  $M_{vir,90}$ . In order to do so, we adopt the calibration presented by Harris et al. (2017), whose validity seems to also extend to the regime of UDGs:

$$\begin{cases} M_{vir} = N_{GC}/\eta_N \\ \eta_N = -8.56 - 0.11 \log M_{vir}/M_\odot \end{cases} \quad (7)$$

Results are listed in Table 1, and correspond to the looses between the upper limits  $N_{GC,90}$  listed in Fig 6 for each UDG. A total of 6 UDGs are compatible with a virial mass between 1 and  $2 \times 10^{11} M_\odot$ , where the latter value represents the upper limit for UDG ID 424. A virial mass equal to or higher than  $10^{11} M_\odot$  can be excluded at 90% for 13 among the 18 largest UDGs in our sample, with  $R_s > 1.5$  kpc.

## 4.2 Analyses on stacks

Results for our 4 stacks, as described in Sect. 3.1.1, are presented in Fig. 5 and Table 1. Panels in Fig. 5 are analogous to those of Fig. 4. The zooms in the left panels display all GCCs, as collected over all UDGs included in the stack.

Color-coding is the same as in Fig. 4, and shows the probability of membership in the UDGs’ GCSs. The right panels display our inferences for the mean properties,  $\langle N_{GC} \rangle$  (on the horizontal axis in units of  $\log \langle N_{GC} \rangle$ ) and  $\langle R_h/R_s \rangle$ . Black crosses extend between the 10% and 90% quantiles of the respective posterior distributions. The blue values in the upper right corner and the vertical grey lines display the reference mean abundance

$$\langle N_{GC,0} \rangle = \frac{1}{n} \sum_j^n (N_{GC,0})_j, \quad (8)$$

where, we recall,  $n$  is the number of UDGs combined in the stack. As in Fig. 4, blue and green ellipses refer to mock datasets with abundances of, respectively,  $1 \times$  and  $2 \times \langle N_{GC,0} \rangle$ .

The stacked CCTp data allow for a much improved statistics on the background counts. Quantile values  $q_i$  listed in Table 1 refer to models with richness that are multiples of the reference mean abundance,  $i \times \langle N_{GC,0} \rangle$ . We find that the model with ‘normal’ abundances  $1 \times N_{GC,0}$  is statistically preferred to a model in which abundances are doubled: for no single stack the center of the black cross falls within the green dashed ellipse, which is drawn to contain the centres for 86% of random realisations of such model with doubles abundances, analysed in the same way as the real data. Furthermore, in all our four stacks the reference expected mean richness  $\langle N_{GC,0} \rangle$  is higher than the median value of the inferred posterior distribution for  $\langle N_{GC} \rangle$ . In one case it is higher than the top 90% quantile, with marginal evidence for somewhat lower mean GC abundances. In fact, the

**Table 1.** Summary of the statistical constraints from our analyses. Column 1 defines the properties of the stacks, or identifies individual UDGs by their ID number, as in the catalogue by Yagi et al. (2016); columns 2 and 3 list stellar scale radii and stellar masses; column 4 collects the GC abundances expected based on the stellar mass of the system, according to eqn. (6);  $q_i = X$  indicates that the UDG is compatible with 100X% of the realisations of a model with the standard value of  $R_h/R_s$  and  $N_{GC} = i \times N_{GC,0}$ ; column 10 uses the loosest between the two upper limits  $N_{GC,90}$  (90% confidence regions) obtained from a Bayesian and a frequentist approach (listed in Fig. 6) to obtain an upper limit of on the virial mass of each halo,  $M_{vir,90}$

stack or ID	$R_S$ kpc	$\log M_*$ $M_\odot$	$N_{GC,0}$	$q_1$	$q_2$	$q_5$	$q_{10}$	$q_x$	$M_{vir,90}$ $10^{10} M_\odot$
$R_S > 1.5$ kpc	1.99	7.64	2.6	0.56	>0.95	>0.95	>0.95	$q_{0.5} = 0.94$	3.04
$R_S \leq 1.5$ kpc	1.03	7.08	1.2	0.83	>0.95	>0.95	>0.95	$q_{1.1} > 0.95$	0.61
$\log M_* > 7.5$	1.80	7.79	2.9	>0.95	>0.95	>0.95	>0.95	$q_{0.5} < 0.39$	0.82
$\log M_* \leq 7.5$	1.13	7.01	1.1	0.55	>0.95	>0.95	>0.95	$q_{1.3} = 0.83$	1.79
<hr/>									
85	0.94	7.18	1.2	<0.39	0.75	>0.95	>0.95	–	2.49
89	1.10	7.50	1.9	0.47	0.47	>0.95	>0.95	–	4.69
91	1.58	6.78	0.7	0.40	0.81	0.94	>0.95	–	1.29
99	2.09	7.22	1.3	0.94	>0.95	<0.39	<0.39	$\{q_{15}, q_{20}\} = \{0.88, >0.95\}$	17.8
102	0.89	7.02	1.0	0.67	0.57	0.86	>0.95	–	3.58
104	1.05	7.30	1.5	0.67	0.88	>0.95	>0.95	–	1.85
105	1.22	6.58	0.6	<0.39	0.72	0.91	>0.95	–	1.63
107	1.99	6.78	0.7	<0.39	0.83	0.91	>0.95	–	1.55
108	0.81	6.58	0.6	<0.39	0.77	>0.95	>0.95	–	0.98
112	1.53	7.74	2.6	<0.39	0.67	>0.95	>0.95	–	6.24
113	0.84	6.38	0.4	<0.39	0.73	0.93	>0.95	–	1.19
114	1.52	7.74	2.6	<0.39	<0.39	0.94	>0.95	–	6.99
115	1.16	6.58	0.6	<0.39	0.50	0.88	>0.95	–	2.09
118	0.88	6.82	0.8	<0.39	0.70	0.94	>0.95	–	3.96
121	1.67	7.82	2.9	0.71	0.88	>0.95	>0.95	–	4.06
122	1.47	7.58	2.1	0.74	0.71	>0.95	>0.95	–	4.76
236	1.25	6.86	0.8	<0.39	<0.39	0.94	>0.95	–	2.09
238	1.06	7.34	1.5	0.74	0.54	>0.95	>0.95	–	3.96
325	1.01	7.02	1.0	<0.39	<0.39	0.92	>0.95	–	3.09
331	1.47	7.58	2.1	<0.39	0.92	>0.95	>0.95	–	2.04
358	1.75	8.10	4.3	0.64	0.46	>0.95	>0.95	–	11.6
366	1.57	7.74	2.6	0.63	0.87	>0.95	>0.95	–	3.94
367	1.48	7.58	2.1	0.55	<0.39	0.86	>0.95	–	8.33
370	3.03	7.66	2.4	<0.39	0.57	0.94	>0.95	–	5.95
372	1.25	7.62	2.2	<0.39	0.54	>0.95	>0.95	–	5.52
373	1.52	7.74	2.6	<0.39	0.63	>0.95	>0.95	–	6.38
374	1.01	7.34	1.5	<0.39	0.74	>0.95	>0.95	–	3.21
380	0.74	6.90	0.9	0.68	0.89	>0.95	>0.95	–	0.94
386	1.93	8.10	4.3	0.66	0.60	>0.95	>0.95	–	11.1
387	1.20	7.66	2.4	0.53	0.88	>0.95	>0.95	–	3.18
391	0.78	6.82	0.8	<0.39	0.87	>0.95	>0.95	–	1.10
395	0.69	6.74	0.7	<0.39	0.69	0.94	>0.95	–	1.42
402	0.77	7.22	1.3	0.40	0.82	>0.95	>0.95	–	2.30
406	1.15	7.18	1.2	0.54	0.80	>0.95	>0.95	–	2.29
407	2.85	8.10	4.3	0.73	0.92	>0.95	>0.95	–	4.33
408	0.82	6.74	0.7	0.60	<0.39	0.65	0.94	–	3.26
409	2.27	7.86	3.1	<0.39	0.82	>0.95	>0.95	–	6.05
410	0.69	7.38	1.6	<0.39	0.59	>0.95	>0.95	–	3.78
412	0.88	7.14	1.2	0.61	0.88	>0.95	>0.95	–	1.45
415	1.10	6.86	0.8	0.45	0.86	>0.95	>0.95	–	1.18
419	1.66	8.10	4.3	0.83	0.64	>0.95	>0.95	–	10.9
421	0.74	6.86	0.8	0.45	0.81	>0.95	>0.95	–	1.38
423	0.77	7.22	1.3	0.42	0.83	>0.95	>0.95	–	2.23
424	1.36	6.70	0.7	>0.95	>0.95	0.93	0.51	$\{q_{30}, q_{40}, q_{45}\} = \{<0.39, 0.80, 0.89\}$	19.8
425	3.11	7.42	1.7	0.65	0.51	0.82	>0.95	–	9.78
427	0.83	6.82	0.8	0.61	0.83	>0.95	>0.95	–	1.22
432	1.10	7.34	1.5	<0.39	0.46	0.94	>0.95	–	3.77
433	1.54	7.14	1.2	0.77	0.74	0.92	>0.95	–	3.66
434	1.38	7.42	1.7	0.47	0.85	>0.95	>0.95	–	2.77
435	0.95	6.74	0.7	>0.95	>0.95	0.88	<0.39	$q_{20} = 0.93$	7.59
436	2.50	7.74	2.6	0.60	<0.39	0.57	>0.95	–	14.75
437	0.77	7.22	1.3	<0.39	0.81	>0.95	>0.95	–	2.37
438	1.45	7.10	1.1	0.46	<0.39	0.81	>0.95	–	4.97
534	1.66	7.78	2.8	<0.39	<0.39	>0.95	>0.95	–	7.43

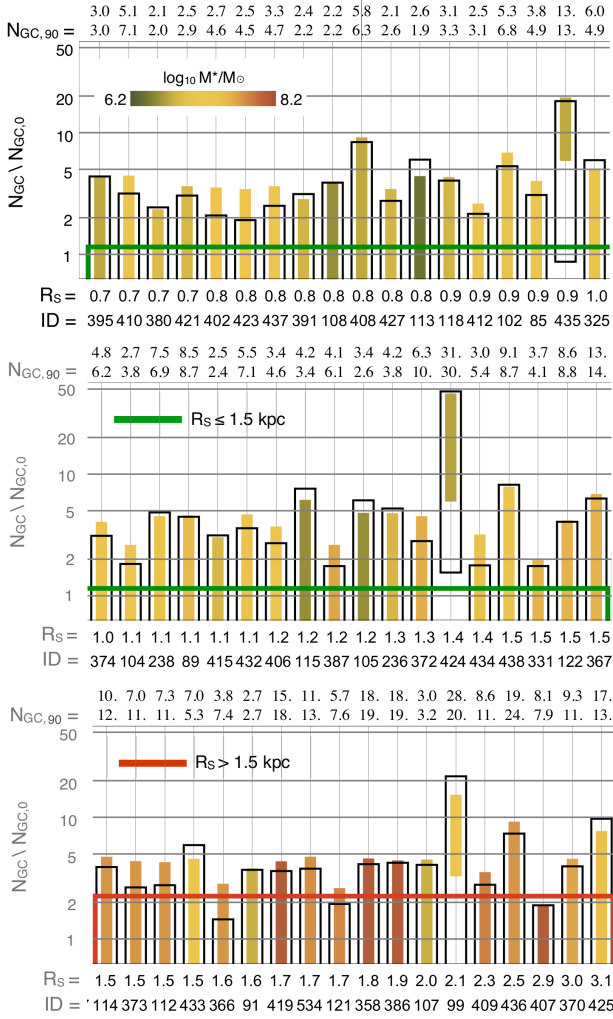


**Figure 6.** Summary of the limits on the richness of the GCS of each of our UDGs, in terms of the mean richness of ‘normal’ dwarf galaxies with the same stellar mass,  $N_{GC}/N_{GC,0}$ . UDGs are ordered by size, and color-coded by stellar masses. Coloured bars refer to limits obtained under the frequentist approach, and display the range of enhancements that would for which 90% of mock realizations would return indistinguishable results. Black empty rectangles extend between the 10% and 90% quantiles of the marginalised posterior distributions, and therefore are associated with a Bayesian interpretation. Results for the mean relative richness  $\langle N_{GC} \rangle / \langle N_{GC,0} \rangle$  obtained from the stacks based on size are displayed as empty coloured rectangles, and show the loosest between these two upper limits.

stack collecting the 18 UDGs with the highest stellar mass,  $\log M_*/M_\odot > 7.5$ , appears to be best compatible with a model with somewhat *lower* abundances than what is ‘normal’.

Between a frequentist and Bayesian interpretation of our result, the loosest upper limit  $\langle N_{GC,90} \rangle$  (90% confidence region) for the stack of the 18 brightest UDGs is  $\langle N_{GC,90} \rangle = 3.7$ . This value implies that an enhancement by a factor  $\gtrsim 1.3$  with respect to the mean GC richness of ‘normal’ dwarfs can be excluded with 90% confidence. The same reasoning for the stack of the 18 largest UDGs provides an upper limit of  $\langle N_{GC,90} \rangle = 5.9$ , which corresponds to a

maximum compatible enhancement of 2.3. The corresponding upper limits for the mean virial masses are respectively  $\langle M_{vir,90} \rangle = 1.8 \times 10^{10} M_\odot$  and  $\langle M_{vir,90} \rangle = 3 \times 10^{10} M_\odot$  for the brightest and largest UDGs, showing once again that most UDGs are puny dwarf galaxies.

## 5 DISCUSSION AND CONCLUSIONS

Our results show that the large majority of UDGs are hosted by dwarf mass haloes. For only five systems in our randomly chosen sample of 54 are GC abundances of  $N_{GC} > 19$  included within the 90% confidence region allowed by the data. The highest upper limit is  $N_{GC,90} = 31$ . In fact, within the sample of the largest 18 UDGs, with  $R_S > 1.5$  kpc, 10 systems have an upper limit of  $N_{GC,90} \leq 11$  with the same confidence. These values are significantly lower than what appropriate for a MW-like halo ( $N_{GC,MW} \approx 144$ , Harris et al. 2017): among our 54 UDGs, all are well within the regime of dwarf galaxies. Corresponding upper limits for the individual halo masses show that only 6 galaxies are compatible with masses between 1 and  $2 \times 10^{11} M_\odot$ . The GCSs of all other 48 UDGs imply a virial mass of  $\lesssim 10^{11} M_\odot$  at 90% confidence.

Beasley & Trujillo (2016) and Peng & Lim (2016) have suggested that, though hosted by dwarf haloes with masses similar to that of the LMC, UDGs might still show signs of ‘failure’, having rich GCSs for their stellar mass. The CCTp data do not support this: our sample of UDGs is perfectly consistent with a population of ‘normal’ dwarf galaxies with the same stellar mass.

These results are summarised in Fig. 7, which explicitly compares the inferred GC abundances of our UDGs with those of nearby galaxies from the compilations of G10 (green stars) and Harris et al. (2013, H13, grey rectangles), as a function of stellar mass<sup>1</sup>. The black solid line represents the relation (6), which, we recall, is a fit to the properties of the sample of nearby dwarf galaxies by Georgiev et al. (2008, 2009, 2010). Note that this includes a minority of galaxies that are not displayed in Fig. 7, as bearing no GCs. Vertical bars (colour-coded by stellar half-light radius) cover the range of GC abundances that are compatible with the CCTp data at 90% confidence. These adopt the loosest between the limits obtained using a Bayesian or a frequentist interpretation, as in Section 4.1.1 and 4.2. Our population of UDGs does not show evidence of deviating from the relation (6), and its scatter around the same relation appears comparable with the one displayed by the ‘normal’ dwarfs in the same Figure. In comparison, coloured rectangles with black edges identify the measurements by Peng & Lim (2016) and Beasley & Trujillo (2016) for DF17, by Beasley et al. (2016) for VCC 1287 in Virgo and by van Dokkum et al. (2016) for DF44. Taken together, the latter set of systems would suggest a mismatch from the properties of either G10 galaxies, H13 galaxies, or our 54 UDGs.

A consistent picture is obtained from the analysis of

<sup>1</sup> For the H13 catalog, stellar masses are obtained using morphological type as a proxy for colour. For our UDGs, the uncertainty displayed in the top-left shows the difference between the masses inferred using the  $M/L$  relations of Zibetti et al. (2009) and Bell et al. (2003).



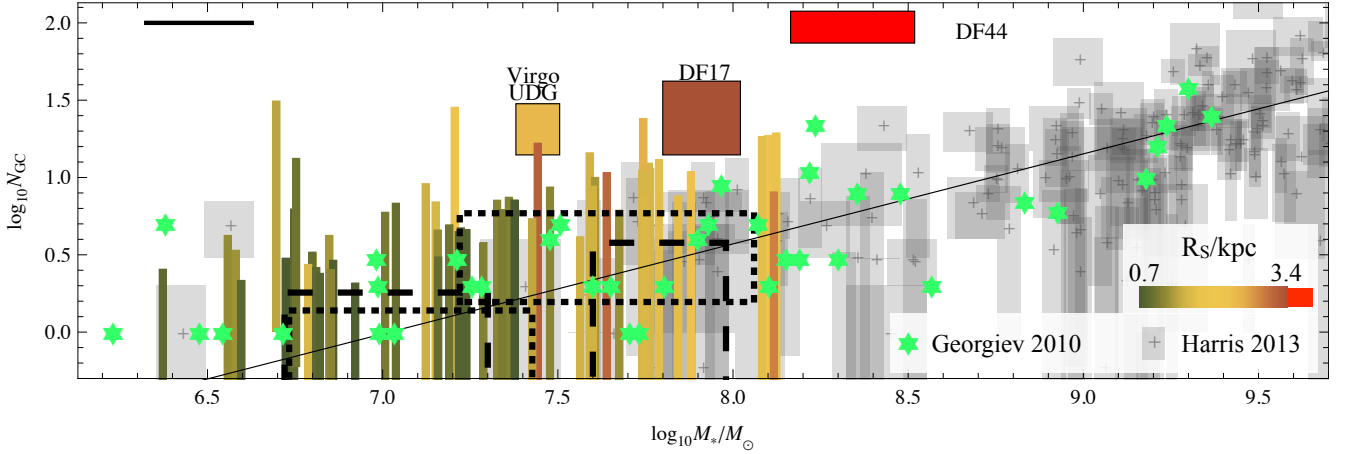


**Figure 7.** The richness of the GCS of ‘normal’ dwarf galaxies, from the H13 catalog (grey rectangles) and from G10 (green stars). The solid black line is a fit to the properties of the dwarf galaxies collected by Georgiev et al. (2008, 2009, 2010), and shown in eqn. (6). Results for all our 54 UDGs (90% confidence regions) are shown as coloured bars, colour-coded by the UDG stellar half-light radius. Literature measurements for UDG GC abundances (two in Coma and one Virgo) are shown as rectangles with a black edge, with the same colour-coding. Dashed empty rectangles display the results of our stacking analyses (mean with  $1\sigma$  scatter for  $\log M_*$ ; 90% confidence regions for the mean GC abundance). Long-dashed rectangles refer to the stacks based on stellar mass. Short dashed rectangles to those based on size.

our stacks. Dashed empty rectangles display these results in Fig. 7: long dashed refers to stacks based on stellar mass, short dashed to stacks based on size. All are in line with the expectation valid for normal dwarf galaxies, if not marginally low. Even within the set of our 18 largest UDGs, a mean enhanced of the GCS richness by a factor  $\gtrsim 2.3$  can be excluded at 90% confidence.

## ACKNOWLEDGEMENTS

NA and AM acknowledge stimulating discussions with Chervin Laporte. NA thanks Adriano Agnello, Mike Beasley and Abraham Loeb for comments on an early version of this draft.

## REFERENCES

Amorisco, N. C., & Evans, N. W. 2011, *MNRAS*, 411, 2118  
 Amorisco, N. C., Evans, N. W., & van de Ven, G. 2014, *Nat*, 507, 335  
 Amorisco, N. C., & Loeb, A. 2016, *MNRAS*, 459, L51  
 Beasley, M. A., Romanowsky, A. J., Pota, V., et al. 2016, *arXiv:1602.04002*  
 Beasley, M. A., & Trujillo, I. 2016, *arXiv:1604.08024*  
 Behroozi, P. S., Wechsler, R. H., & Conroy, C. 2013, *ApJ*, 770, 57  
 Bell, E. F., McIntosh, D. H., Katz, N., & Weinberg, M. D. 2003, *ApJS*, 149, 289  
 Bellazzini, M., Belokurov, V., Magrini, L., et al. 2017, *MNRAS*, 466, 42  
 Caldwell, N., & Romanowsky, A. J. 2016, *ApJ*, 824, 42  
 Campbell, D. J. R., Frenk, C. S., Jenkins, A., et al. 2016, *arXiv:1603.04443*  
 Di Cintio, A., Brook, C. B., Dutton, A. A., et al. 2016, *arXiv:1608.01327*  
 Forbes, D. A., Alabi, A., Romanowsky, A. J., et al. 2016, *MNRAS*, 458, L44  
 Georgiev, I. Y., Goudfrooij, P., Puzia, T. H., & Hilker, M. 2008, *AJ*, 135, 1858–1876

Georgiev, I. Y., Puzia, T. H., Hilker, M., & Goudfrooij, P. 2009, *MNRAS*, 392, 879  
 Georgiev, I. Y., Puzia, T. H., Goudfrooij, P., & Hilker, M. 2010, *MNRAS*, 406, 1967  
 Guo, Q., White, S., Li, C., & Boylan-Kolchin, M. 2010, *MNRAS*, 404, 1111  
 Hammer, D., Verdoes Kleijn, G., Hoyos, C., et al. 2010, *ApJS*, 191, 143  
 Harris, W. E., Harris, G. L. H., & Alessi, M. 2013, *ApJ*, 772, 82  
 Harris, W. E., Harris, G. L., & Hudson, M. J. 2015, *ApJ*, 806, 36  
 Harris, W. E., Blakeslee, J. P., & Harris, G. L. H. 2017, *ApJ*, 836, 67  
 Hudson, M. J., Harris, G. L., & Harris, W. E. 2014, *ApJL*, 787, L5  
 Jordán, A., McLaughlin, D. E., Côté, P., et al. 2007, *ApJS*, 171, 101  
 Kartha, S. S., Forbes, D. A., Spitler, L. R., et al. 2014, *MNRAS*, 437, 273  
 Koda, J., Yagi, M., Yamanoi, H., & Komiyama, Y. 2015, *ApJL*, 807, L2  
 Mackey, A. D., & Gilmore, G. F. 2003, *MNRAS*, 338, 85  
 Martinez-Delgado, D., Laesker, R., Sharina, M., et al. 2016, *arXiv:1601.06960*  
 Mihos, J. C., Durrell, P. R., Ferrarese, L., et al. 2015, *ApJL*, 809, L21  
 Miller, B. W., & Lotz, J. M. 2007, *ApJ*, 670, 1074  
 Moster, B. P., Naab, T., & White, S. D. M. 2013, *MNRAS*, 428, 3121  
 Muñoz, R. P., Eigenthaler, P., Puzia, T. H., et al. 2015, *ApJL*, 813, L15  
 Peng, E. W., Jordán, A., Blakeslee, J. P., et al. 2009, *ApJ*, 703, 42  
 Peng, E. W., Ferguson, H. C., Goudfrooij, P., et al. 2011, *ApJ*, 730, 23  
 Peng, E. W., & Lim, S. 2016, *ApJL*, 822, L31  
 Plummer, H. C. 1911, *MNRAS*, 71, 460  
 Roman, J., & Trujillo, I. 2016, *arXiv:1603.03494*  
 Salinas, R., Alabi, A., Richtler, T., & Lane, R. R. 2015, *AA*, 577, A59  
 Schlafly, E. F., & Finkbeiner, D. P. 2011, *ApJ*, 737, 103  
 Schlegel, D. J., Finkbeiner, D. P., & Davis, M. 1998, *ApJ*, 500,

525

- Sirianni, M., Jee, M. J., Benítez, N., et al. 2005, *PASP*, 117, 1049
- Trujillo, I., Román, J., Filho, M., & Sánchez Almeida, J. 2017, arXiv:1701.03804
- van der Burg, R. F. J., Muzzin, A., & Hoekstra, H. 2016, arXiv:1602.00002
- van Dokkum, P. G., Abraham, R., Merritt, A., et al. 2015, *ApJL*, 798, L45
- van Dokkum, P., Abraham, R., Brodie, J., et al. 2016, *ApJL*, 828, L6
- Yagi, M., Koda, J., Komiyama, Y., & Yamanoi, H. 2016, *ApJS*, 225, 11
- Yozin, C., & Bekki, K. 2015, *MNRAS*, 452, 937
- Walker, M. G., Mateo, M., Olszewski, E. W., et al. 2009, *ApJ*, 704, 1274
- Walker, M. G., & Peñarrubia, J. 2011, *ApJ*, 742, 20
- Wolf, J., Martinez, G. D., Bullock, J. S., et al. 2010, *MNRAS*, 406, 1220
- Zaritsky, D., Crnojević, D., & Sand, D. J. 2016, *ApJL*, 826, L9
- Zaritsky, D. 2016, arXiv:1609.08169
- Zibetti, S., Charlot, S., & Rix, H.-W. 2009, *MNRAS*, 400, 1181